ACS OMEGA

http://pubs.acs.org/journal/acsodf

Article

Highly Sensitive NO_2 Detection by TVS-Grown Multilayer MoS_2 Films

Kenjiro Hayashi,* Masako Kataoka, Hideyuki Jippo, Junichi Yamaguchi, Mari Ohfuchi, and Shintaro Sato*

Cite This: *ACS Omega* 2022, 7, 1851−1860

Read Online

ACCESS | Metrics & More | Article Recommendations | Supporting Information

ABSTRACT: Two-dimensional layered materials have been investigated for sensor applications over the last decade due to their very high specific surface area and excellent electrical characteristics. Although grain boundaries are inevitably present in polycrystalline-layered materials used for real applications, few studies have investigated their effects on sensing properties. In this study, we demonstrate the growth of two distinct MoS_2 films that differ in grain size by means of chemical vapor deposition (CVD) and thermal vapor sulfurization (TVS) methods. Transistor-based sensors are fabricated using these films, and their NO_2 sensing properties are evaluated. The adsorption behavior of NO_2 on MoS_2 is considered in terms of the Langmuir isotherm, and the experimental results can be well fitted by the equation. The CVD-grown film exhibits electrical properties 1−2 orders of magnitude superior to those of the TVS-grown one, which is attributed to the large grain size of the CVD-grown film. In contrast, the sensitivity to NO_2 is unexpectedly found to be higher in the TVS-grown film and is of the same order of a previously reported record value. Transmission electron microscopy observations suggest that the TVS-grown film consists of multiple rotationally oriented grains that are connected by mirror twin grain boundaries. Theoretical calculation results reveal that the adsorption of NO_2 on the grain boundary that we modeled is equal to that on the ideal basal plane surface of MoS_2. In addition, the porous structure in the TVS-grown film may also contribute to enhancing the sensor response to NO_2. This study suggests that a highly sensitive MoS_2 sensor can also be fabricated by using a polycrystalline film with small grain size, which can possibly be applied to other two-dimensional materials.

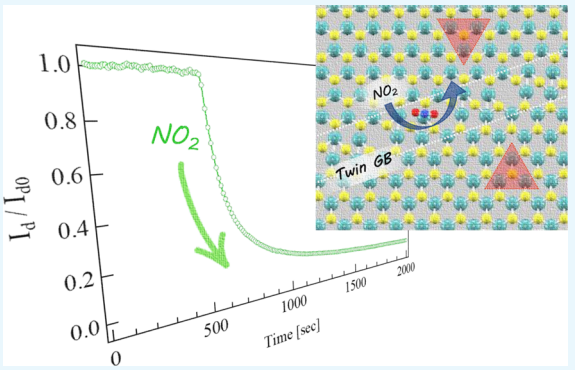

INTRODUCTION

Two-dimensional materials have attracted attention over the years from researchers in various fields owing to their unique properties. Among them, metal chalcogenides are expected to be good candidates for electronic devices since they exhibit a wide variety of electronic and optical properties in accordance with their elemental composition and crystal structure.[1] Molybdenum disulfide (MoS_2) has also been widely studied for its great potential in a field effect transistor (FET).[2,3] In addition to the high on/off current ratio and moderate electron mobility, the FET shows electric responses upon exposure to specific gas species, which has been the motivation for studying its potential as a material in sensor applications.[4−7] The MoS_2 films used in highly sensitive nitrogen oxide (NO_2) sensors are usually prepared by the exfoliation of bulk crystal or chemical vapor deposition (CVD).[8−11] However, these methods have difficulties in terms of thickness control and film uniformity that significantly affect the device fabrication yield. On the other hand, thermal vapor sulfurization (TVS), in which MoS_2 is grown by heating a metallic Mo film in a sulfur vapor environment, has advantages in terms of the above-mentioned problems because the thickness and uniformity of the resulting MoS_2 film are basically determined in accordance with the initial geometry of the pre-deposited Mo film.[12,13] Therefore, the TVS-grown film is likely to be compatible with the mass production of MoS_2 devices. However, it typically shows relatively poor electric properties due to its small grain size. Specifically, it has a considerably denser grain boundary (GB) than the CVD-grown film. Although such films that possess polycrystalline nature seem to lack the potential to be used in a low-ppb (parts per billion) NO_2 detectable sensor, few studies have examined the sensing performance of TVS-grown films.[14]

In this study, we fabricate an FET-based sensor using the TVS-grown MoS_2 film and evaluate its electric properties and sensor response to NO_2 gas for comparing its sensing ability with that of the CVD-grown film. Although most of the previous research has focused on the NO_2 adsorption behavior only on the ideal basal plane surface of MoS_2 to explain the sensor response, the effect of grain boundaries in MoS_2 films is

Received: September 15, 2021
Accepted: November 25, 2021
Published: January 4, 2022

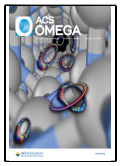

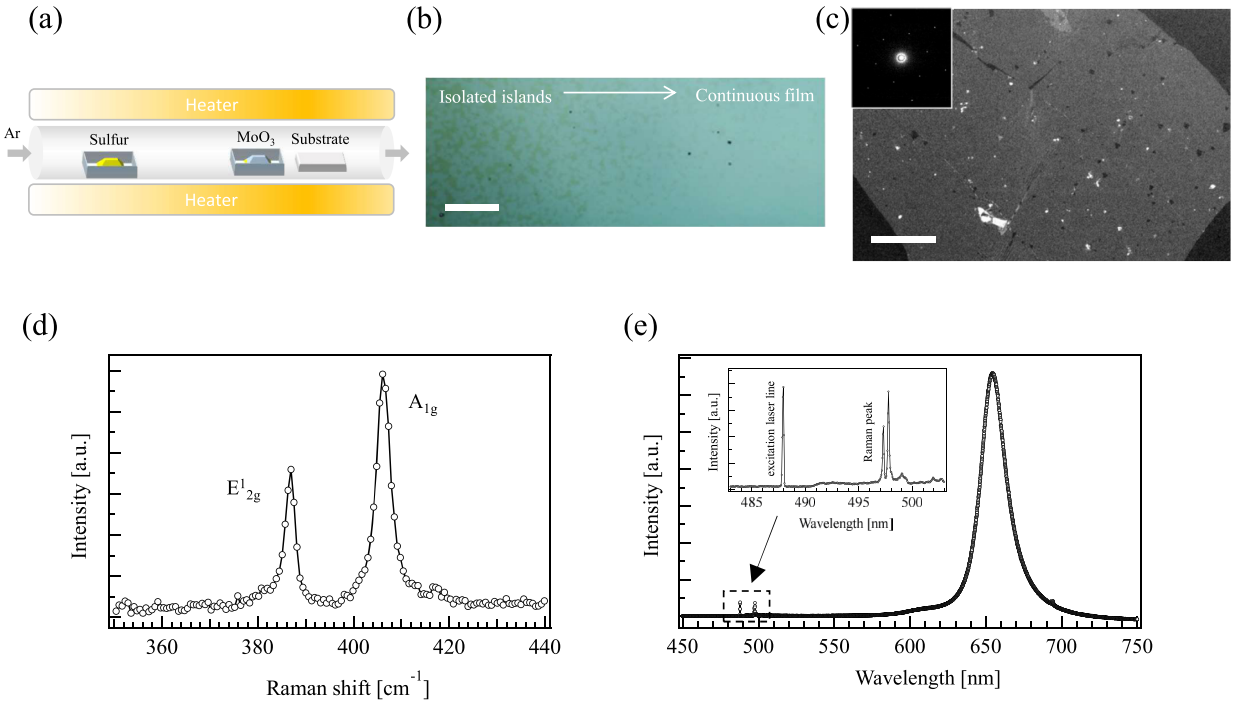

Figure 1. (a) Schematic illustration of the CVD growth furnace setup. The substrate and MoO_3 powder are placed in a heating zone, and sulfur is placed upstream from the substrate. (b) Optical microscopy image of the MoS_2 film grown on the substrate. (c) Dark-field TEM image of a CVD-grown MoS_2 film. The inset shows the corresponding SAED pattern. Scale bars shown in (b,c) are 50 μm and 500 nm, respectively. (d,e) Raman and PL spectra of the CVD-grown MoS_2 film taken on the growth substrate. The inset in (e) is a magnified image of Raman peaks.

still unrevealed. In this regard, it is important to investigate the sensing ability of polycrystalline MoS_2 containing a large amount of GB that would inevitably be present in the film while fabricating a sensor for practical use. To evaluate the net sensor response to low-ppb NO_2, the drain current change when exposed to NO_2 is measured in a nitrogen (N_2) atmosphere for excluding the effect of oxygen and humidity on the sensing properties. In addition, all electrical measurements are conducted in a stainless steel chamber under dark conditions to avoid extrinsic effects induced by light illumination that can cause photocurrent generation[15,16] and desorption of adsorbed gas molecules on the MoS_2 surface.[17,18] The TVS-grown film is found to have lower electrical properties than the CVD-grown film. Contrary to our expectation, however, the TVS-grown film shows higher response to NO_2 than the CVD-grown film. The sensor exhibits clear response to NO_2 with concentrations as low as 7 ppb and more than 90% change in drain current without any contribution of the extrinsic effect, whose responsivity is of the same order as a previously reported record value achieved with the support of light illumination.[19,20] To verify this interesting finding, we then demonstrate transmission electron microscopy (TEM) observations to investigate the grain structure of the TVS-grown film. The film is suggested to be polycrystalline, although it consists of well-aligned grains with mirror twin GBs. Theoretical calculations are performed to evaluate the adsorption behavior of NO_2 on the MoS_2 surface with and without the GB. The results reveal that the adsorption energy on the GB is estimated to be comparable to that on the ideal MoS_2 surface. Furthermore, the porous structure found in the film possibly contributes to enhancing the NO_2 adsorption properties. These results suggest that the highly crystalline film with a large grain size is not essential to improve the sensing performance of a MoS_2-based sensor. This is rather favorable to sensor fabrication considering that the TVS method can synthesize a wafer-scale MoS_2 film with uniform thickness at a relatively low cost. Our findings can help to clarify the mechanisms underlying NO_2 sensing by MoS_2 films and expand the strategies for developing an ultrasensitive chemical sensor utilizing two-dimensional materials.

METHODS

MoS_2 Growth. MoS_2 growth was performed in a quartz tube furnace where three heating zones can be controlled independently. $Al_2O_3(0001)$ substrates (sapphire C-face wafer) with mirror-polished surfaces were used for growth substrates. Prior to the growth, three cycles of Ar gas flushing followed by evacuation were carried out to reduce the concentration of residual oxygen in the furnace.

CVD growth was demonstrated under atmospheric pressure with 500 sccm (standard cubic centimeters per minute) of Ar used as a carrier gas. A continuous film of single-layer MoS_2 was successfully synthesized on the sapphire substrate. MoO_3 powder (99.95%) and high-purity elemental sulfur (99.9999%) were used as precursors. The growth setup is schematically illustrated in Figure 1a. The sulfur source is placed in the furnace upstream from MoO_3 and the substrate where the temperature is controlled at around 140−180 °C during growth. The substrate is located downstream next to a MoO_3-contained quartz boat. The growth zone temperature was 800 °C, at which the evaporated MoO_3 reacts with the sulfur vapor, resulting in the formation of a MoS_2 film on the surface of the substrate.

TVS growth was conducted in the same furnace used for CVD. The Mo film (1.0 nm thick) was deposited on sapphire substrates at room temperature. The Mo source was evaporated by electron bombardment (EB) in a high-vacuum

https://doi.org/10.1021/acsomega.1c05113
ACS Omega 2022, 7, 1851−1860

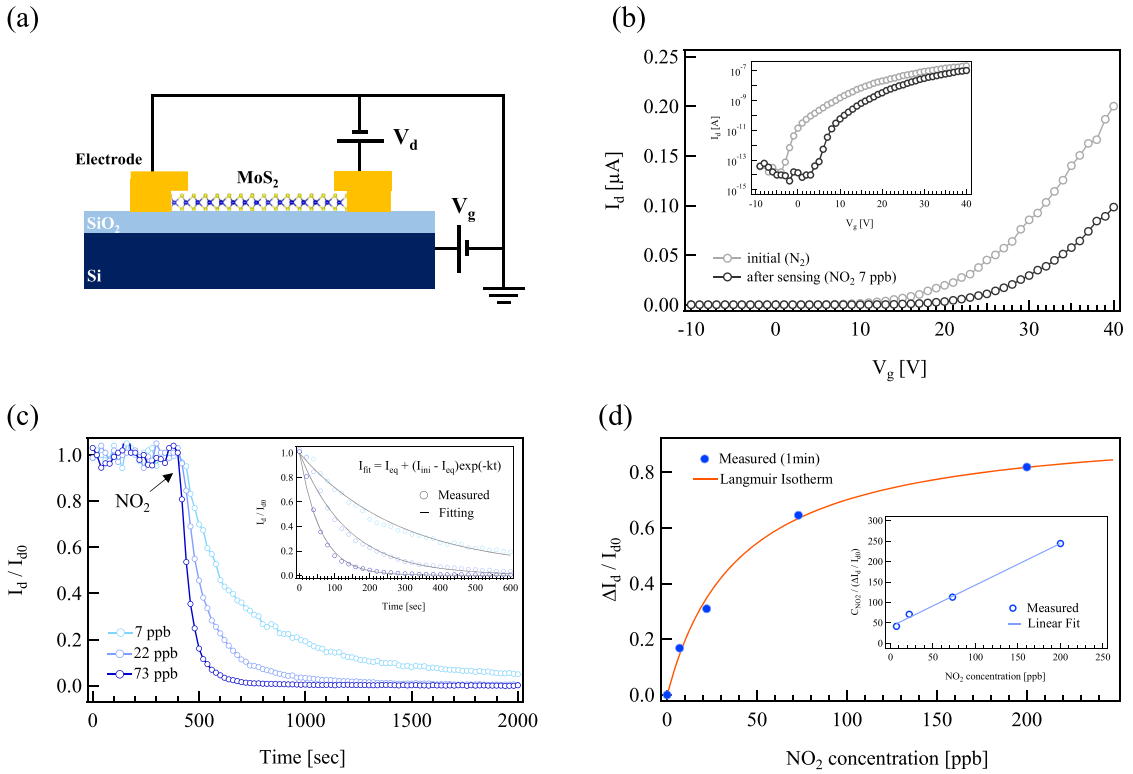

Figure 2. (a) Schematic illustration of an FET-based MoS_2 sensor (V_d: drain voltage, V_g: gate voltage). (b) Drain current (I_d) as a function of V_g of a CVD-grown MoS_2 FET with a channel length of 4 μm. The V_d was 1 V. The inset shows the $I_d - V_g$ curve displayed with the logarithmic axis. (c) Normalized I_d of the CVD-grown MoS_2 sensor when exposed to 7, 22, and 73 ppb of NO_2. The inset shows the corresponding fitted curves. (d) Sensor response ($(\Delta I_d/I_{d0})$ after 1 min exposure to NO_2 plotted as a function of the concentration with the fitted curve using the Langmuir isotherm equation. The inset shows the corresponding linear fitting of the measured data.

chamber. The elemental sulfur was used for Mo sulfurization. The Mo sample and the sulfur placed in a quartz boat were introduced into the furnace. The sample was first annealed at 300 °C for 30 min in a diluted H_2/Ar mixture at atmospheric pressure to reduce native oxides on the Mo film. Then, the sample temperature was elevated up to 1000 °C with an Ar flow of 500 sccm. Meanwhile, the temperature of sulfur, which was placed upstream from the Mo sample, was also raised to 140 °C. After annealing the sample for 30 min, the growth temperature was maintained at 1000 °C, and the furnace was then cooled down under constant Ar flow.

Device Fabrication and Characterization Methods. After the growth, the MoS_2 film was transferred onto a Si substrate with a 90 nm-thick thermal SiO_2 layer by the conventional polymethyl methacrylate (PMMA) transfer method for back-gated FET fabrication.[21] Standard photolithography followed by oxygen plasma reactive ion etching was used to pattern the MoS_2 film. The Ti/Au (10/50 nm) source and drain electrodes were deposited by EB evaporation. The typical channel length of the MoS_2 FET is around several micrometers. All electrical measurements were performed using a semiconductor parameter analyzer (Agilent 4156C). Unless otherwise noted, two-terminal $I-V$ (current−voltage) curves were measured for the MoS_2 FETs in a N_2 atmosphere at room temperature after thermal annealing at 200 °C under vacuum to evaluate the electric properties of the native MoS_2 film. A sensing test was demonstrated using a home-built apparatus that is described in detail elsewhere.[22] Diluted NO_2 was used as a test gas for carrying out measurements using the calibration gas generating equipment (GASTEC PD-1B). The sensing test was performed by monitoring the drain current of the FET-based sensor while NO_2 was supplied. The back-gate bias was set to the value where the drain current was in the subthreshold region. The samples were annealed under vacuum conditions before every measurement to refresh the sensor. All measurements are conducted at room temperature under dark conditions to avoid light illumination effects on MoS_2.

Photoluminescence (PL) and Raman spectroscopies (Horiba Jobin Yvon LabRAM HR-800) were performed at room temperature to confirm MoS_2 formation with an excitation laser wavelength of 488 nm. X-ray photoelectron spectroscopy (XPS) was performed at room temperature using a Kratos AXIS-HSi system equipped with monochromatized Al Kα radiation source (photon energy 1486.6 eV). TEM and scanning TEM (STEM) images were taken at an acceleration voltage of 80 or 200 kV with an FEI Tecnai Osiris. The TEM specimens were prepared using a holey carbon gold grid by means of the above-mentioned transfer method.

Theoretical Calculations. Electronic structure calculations were performed using the first-principles calculation code, PHASE.[23] The exchange−correlation potential was treated with generalized gradient approximation (GGA) using the Perdew−Burke−Ernzerhof functional.[24] To describe the long-range interaction, the vdW-D2 method was adopted to include the van der Waals interactions.[25] Valence electrons are generated in Mo $4p^6 4d^5 5s^1$ and S $3s^2 3p^4$ configurations. The cutoff energies were set on 25 Ryd for plane-wave expansion and 230 Ryd for integration of charge density in real

https://doi.org/10.1021/acsomega.1c05113
ACS Omega 2022, 7, 1851−1860

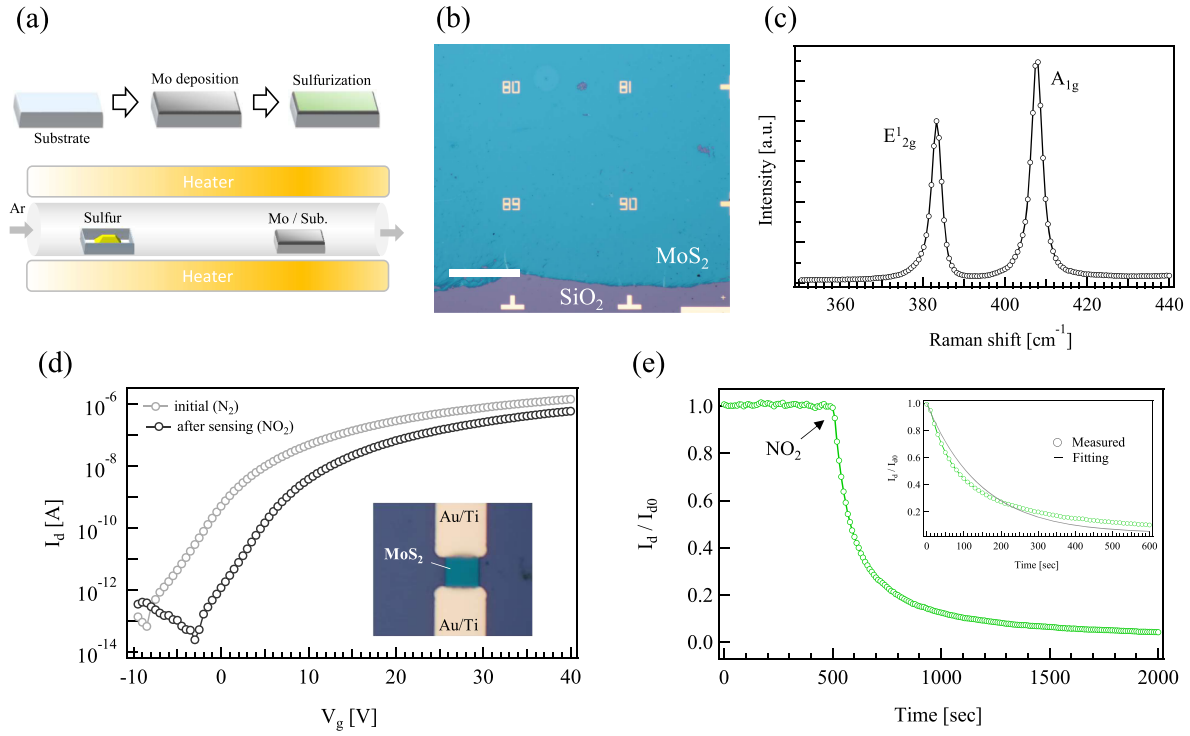

Figure 3. (a) Schematic illustration of the growth procedure and furnace setup for the TVS method. The substrate is placed in a heating zone, and sulfur is placed upstream from the substrate. (b) Optical microscopy image of the TVS-grown MoS_2 film after being transferred onto a Si/SiO_2 substrate. The scale bar is 300 μm. (c) Raman spectrum of the TVS-grown MoS_2 film taken on the growth substrate. (d) I_d as a function of V_g of a TVS-grown MoS_2 FET with a channel length of 4.5 μm. The V_d was 1 V. (e) Normalized I_d of the TVS-grown MoS_2 sensor when exposed to 7 ppb of NO_2. The inset shows the corresponding fitted curves.

space. The Bader charge analysis was carried out to evaluate the charge transfer from the MoS_2 surface to a NO_2 molecule.

RESULTS AND DISCUSSION

CVD-Grown MoS_2 Film. The schematic of the experimental setup for CVD growth is shown in Figure 1a. The MoS_2 film is synthesized in a quartz tube furnace where MoO_3 powder and elemental sulfur crystal are used as source materials (see Methods for details). Figure 1b shows an optical microscopy image of the MoS_2 film grown on the sapphire substrate. MoS_2 forms triangular islands, and their coverage increases to the right in the image, merging to form a continuous film. Previous studies have also reported that the CVD method has difficulty in precisely controlling the uniformity of growth coverage and the thickness of the MoS_2 film.[26,27] The film in the full-coverage region is characterized by TEM analysis to evaluate the grain size of the CVD-grown MoS_2 since it will be utilized for fabricating sensor devices as described later. A dark-field TEM image and the corresponding selected area electron diffraction (SAED) pattern in the inset are shown in Figure 1c. The typical grain size is found to range from 3 to 5 μm from the TEM observations where a single grain appears as a bright region in the image. Raman and PL spectroscopies are performed to analyze the layer number and crystallinity of the CVD-grown film. The Raman spectrum shows two prominent peaks at 387 and 406 cm^{-1}, which correspond to the E^1_{2g} and A_{1g} modes of MoS_2.[28] As shown in Figure S1a, no obvious Raman features related to structural defects in MoS_2 are seen in the low-wavenumber region of the spectrum.[29] The full widths at half-maximum (FWHMs) are extracted by fitting the E^1_{2g} and A_{1g} peaks and are estimated to be 2.47 and 3.43 cm^{-1} (see Figure S1), respectively, indicative of the crystallinity of MoS_2 being higher than in previous reports.[30,31] Furthermore, the layer number of the film is identified as a single layer from a distance of 19.1 cm^{-1} between the two peaks.[32,33] The film also shows a strong PL peak at 655 nm whose intensity is considerably higher than those of Raman peaks as shown in the inset of Figure 1e, which is due to the direct optical band gap inherent in single-layer MoS_2, supporting the result of Raman spectroscopy.

After transferring the CVD-grown film onto a Si/SiO_2 substrate, back-gated FETs were fabricated in a standard photolithography process. Note that the typical MoS_2 channel size of the FET is around several micrometers in length, which is almost the same as the grain size. Before electrical measurement, the samples were first annealed under vacuum to eliminate the effect of surface adsorbates such as H_2O and O_2 molecules on the electrical properties of the FETs. Unless otherwise noted, all measurements were carried out in a N_2 atmosphere under dark conditions at room temperature in a two-probe configuration. The FETs typically exhibit an n-type semiconducting behavior as can be seen in Figure 2b.[34] The electron mobility of the FET reached 14.9 $cm^2\ V^{-1}\ s^{-1}$ with a current on/off ratio of more than 10^7, which compares favorably with the reported values.[35,36] Then, the sensing properties of the FET-based sensor are tested by measuring the change in drain current value when exposed to various concentrations of NO_2. Figure 2c shows the normalized drain current (I_d/I_0) of the sensor with time for 7, 22, and 73 ppb NO_2 exposure. The NO_2 exposure leads to a rapid decrease in drain current in which the slope becomes steeper as the concentration increases. Responses to NO_2 and other gas species were also measured to evaluate the selectivity as shown

https://doi.org/10.1021/acsomega.1c05113
ACS Omega 2022, 7, 1851−1860

in Figure S2, which is key to the gas sensor. The threshold voltage shift in the positive direction is clearly observed in the $I-V$ curves obtained before and after NO_2 exposure as can be seen in Figure 2b, which explains the above-mentioned drain current change and corresponds to hole doping by NO_2. The sensor response ($\Delta I_d/I_{d0}$) after 1 min exposure to NO_2 is plotted as a function of concentration in Figure 2d. If it is assumed that the response depends on the NO_2 coverage on the MoS_2 surface, the sensing behavior relative to the NO_2 concentration (C_{NO2}) is explained by the Langmuir isotherm equation. The obtained response values are fairly fitted by the equation curve. The plot of $C_{NO_2}/(\Delta I_d/I_{d0})$ on the concentration in the inset of Figure 2d also agrees with linear fitting, which is another expression of Langmuir isotherm, further illustrating the stability and repeatability of the sensor. This result also indicates either that the coverage of the adsorbed NO_2 molecules cannot exceed one monolayer on the MoS_2 surface or that even if the molecules form the second and subsequent adlayers on the surface, they do not contribute to the hole doping to MoS_2. This suggests that the doping is caused by charge transfer from NO_2 that directly adsorbs on MoS_2 as will be discussed later. Here, NO_2 adsorption on the MoS_2 surface can be described as the following reaction equation: $S_{free} + NO_2 \rightleftarrows S_{NO_2}$ (S_{NO_2} and S_{free} denote the site on the MoS_2 surface with and without an adsorbed NO_2 molecule, respectively). Assuming that the NO_2 gas is constantly supplied in the sensing chamber, the above equation can be written as $S_{free} \rightleftarrows S_{NO_2}$. Based on the first-order reversible reaction model, the drain current during the sensor response to NO_2 gas follows $I = I_{eq} + (I_{ini} - I_{eq})\exp(-kt)$, in which I_{ini} and I_{eq} are initial and equilibrium values of the drain current, respectively, k is the rate constant, and t is the elapsed time.[37] The fitted curves match the measured data well as shown in the inset of Figure 2c, and the rate constants are determined to be 0.0035 for 7 ppb, 0.0072 for 22 ppb, and 0.0165 for 73 ppb. The sensor shows a clear response to NO_2 with a concentration as low as 7 ppb and exhibits more than 90% change in the drain current. Since the signal-to-noise (S/N) ratio is estimated to be ~35, a 1 ppb or lower concentration of NO_2 could be detected. However, the sensor after the measurement could barely recover its original property at room temperature even when exposed to N_2, consistent with sensors reported elsewhere.[8−10] This implies that NO_2 molecules are strongly adsorbed on the MoS_2 surface. In this regard, photo-induced effects by light illumination on the sensor have been suggested to improve the recovery speed.[38,39]

TVS-Grown MoS_2 Film. Next, we evaluate the sensor utilizing the TVS-grown film. The MoS_2 film is synthesized by sulfurizing the thin Mo film at an elevated temperature. After Mo film deposition, the sample was introduced into the quartz tube furnace. The growth process is schematically illustrated in Figure 3a. The Mo film reacting with vaporized sulfur at an elevated temperature gives rise to the MoS_2 film where the number of layers varies accordingly depending on the thickness of the pre-deposited Mo film. An optical microscopy image of MoS_2 transferred onto a pre-patterned SiO_2/Si substrate shows a continuous film with uniform color contrast over the millimeter-scale range. The Raman spectrum of the as-grown MoS_2 film is shown in Figure 3c. Two prominent peaks of MoS_2 are clearly observed. The separation between the peaks is estimated to be 24.1 cm^{-1}, indicating multilayer MoS_2 that consists of four to five layers.[32,33] The peak located at 286 cm^{-1} as shown in Figure S3a appears when the film is a multilayer MoS_2.[40] The LA(M) peak at ~227 cm^{-1} is not visible in the spectrum. This is reported to be most prominent among the peaks that are induced by defects in MoS_2, whose intensity is proportional to the density of the defects. Although the faint defect-induced peaks (150−200 cm^{-1}) are visible,[29] their intensity is fairly low compared to the two prominent E^1_{2g} and A_{1g} peaks. As will be described later, these would be attributed to a certain number of structural defects present at twin GBs in the TVS-grown film. The stacking order of the film is found to be 2H phase, which is deduced from the Raman feature where the vibration modes of the 1T phase are barely seen.[41] Since the FWHM of the E^1_{2g} mode is known to be relatively insensitive to the number of layers,[42] it could be used as an index for comparing the crystalline quality. The FWHM values of E^1_{2g} and A_{1g} of our film are found to be 3.0 and 3.2, respectively (Figure S3), which are narrower than previously reported values taken from TVS-grown films.[43−46] Furthermore, single-layer MoS_2 films grown by CVD have exhibited the values in the range of 3.2−3.8 for E^1_{2g} and 3.7−6.8 cm^{-1} for A_{1g},[47−49] suggesting that the crystalline quality of our TVS-grown film is comparable to that of the CVD-grown films in the previous reports. The chemical composition of the MoS_2 film was characterized by XPS (see Figure S4). The elemental ratio S/Mo of the TVS-grown film was found to be ~2.1, which is almost equal to the value of the CVD-grown film (data not shown). This is indicative of the fact that the amount of sulfur vacancies in the films is negligible, which is consistent with the results of Raman measurement that showed high crystallinity of the TVS-grown film. Therefore, the contribution of the vacancies to NO_2 sensing is considered to be fairly small.

The MoS_2 FETs were fabricated on a SiO_2/Si substrate to characterize their electronic properties. First, room-temperature $I-V$ curves are measured for all devices fabricated to evaluate the electrical properties of the TVS-grown film. All the FETs exhibit an n-type semiconducting behavior, as observed in our CVD-grown film. The $I-V$ curves measured in an air atmosphere (not shown) exhibited electron mobilities ranging from 0.1 to 3.0 $cm^2\ V^{-1}\ s^{-1}$ at maximum and a current on/off ratio of 10^5-10^6, which are larger than the previously reported values of the TVS-grown film.[50,51] Note that their values can be further improved by measuring the devices in an inert atmosphere where MoS_2 can avoid unintentional counter-doping induced by the absorbed H_2O and O_2 molecules.[52−54] The MoS_2 film synthesized from the Mo film with thickness thinner than 1 nm exhibits higher electric resistance (not shown), which may be due to the insufficient surface coverage and/or the small grain size of MoS_2. Mo film evaporation from the substrate surface at the growth temperature leads to reduced MoS_2 film thickness. Also, in contrast to layer-by-layer growth for CVD,[55] TVS gives rise to multilayer MoS_2 grains before the lateral growth completes the formation of the continuous layer, which leads to a distribution in the number of layers of the resultant film.[13] Figure 3d shows a typical $I-V$ curve of the sensor measured in a N_2 atmosphere after vacuum annealing. The electron mobility and the on/off ratio of the FET were 2.2 $cm^2\ V^{-1}\ s^{-1}$ and 10^7, respectively. Then, we examine the gas sensing property of the TVS-grown MoS_2 sensor. The sensor is found to detect NO_2 with concentrations as low as 7 ppb and exhibited resistivity change by an order of magnitude, as shown in Figure 3e. The repeatability of the sensor was confirmed by obtaining $I-V$ curves before and after

https://doi.org/10.1021/acsomega.1c05113
ACS Omega 2022, 7, 1851−1860

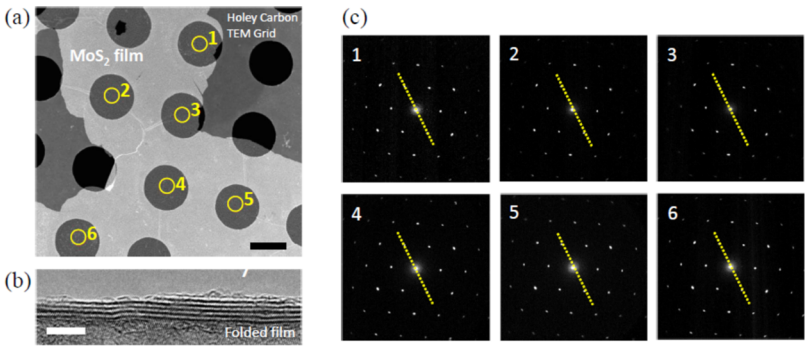

Figure 4. (a) TEM image of a TVS-grown MoS_2 film transferred onto a holey carbon TEM grid. (b) TEM image taken at the edge of a folded film. (c) SAED patterns taken at the corresponding areas marked in (a). Scale bars shown in (a,b) are 2 μm and 5 nm, respectively.

the recovery. As can be seen from Figure S5, the $I-V$ characteristics of the sensor after thermal annealing are completely returned to that of the initial state. The curve fitting of the sensor response as shown in the inset of Figure 3e was found to be deviated from the experimental data. As will be mentioned later, this deviation may be due to the presence of GBs or edges on the TVS-grown film where the adsorption property could differ from that on an ideal surface. However, the rate constant derived from the fitting curve reached 0.0069, which is almost twice the value of the CVD-grown film, which is indicative of having higher sensitivity than the CVD-grown film. Therefore, NO_2 with a concentration of several hundreds of ppt (parts per trillion) or lower would probably be detectable. This is comparable in NO_2 sensitivity to recent reports where the detection limit reached 100 ppt. It is noteworthy that our result is obtained at room temperature under dark conditions, while the above record value was achieved with the assistance of the extrinsic effects caused by red light illumination[19] or forming MoS_2/ZnO nanocomposites in addition to near-infrared light illumination.[20] The sensor performances of the MoS_2-based sensors for NO_2 detection reported in previous studies are listed in Table S1. This is unexpected for the TVS-grown film, which usually exhibits inferior electronic properties to the exfoliated and CVD-grown ones. The typical size of the MoS_2 grain of the TVS-grown film is in the range of several tens of nanometers,[12,46] which is 2 orders of magnitude smaller than that of the CVD-grown film. Considering the channel length of the FET, a significant amount of GB is probably present on the surface of the MoS_2 sensor. Although the adsorption properties of gas molecules could be affected by GBs where the atomic structure is distorted, to the best of our knowledge, there have been no studies addressing this.

The TEM observation was then performed to characterize the grain structure in the TVS-grown film. The TEM sample was prepared by the conventional PMMA transfer process as described in the Methods section. Figure 4a shows the TEM image of the sample where the bright area corresponds to the MoS_2 film transferred on the grid. A folded part observed at the film edge clearly shows that the film consists of four to five layers as can be seen in Figure 4b, which is consistent with the results of Raman spectroscopy. The 2H phase of MoS_2 is confirmed again by observing the honeycomb lattice structure as shown in Figure S6, which is characteristic of the 2H stacking.[56] The SAED patterns obtained at the corresponding spots marked by circles exhibit a single set of hexagonal spots originated from a crystal structure of MoS_2, indicating that the film grew laterally on the substrate and contains no rotational grain in the spot area (spot size: 1 μm). Furthermore, all the SAED patterns are found to be oriented in the same direction as displayed by the dashed lines. Note that the SAED patterns obtained at the areas located 0.5 mm or more apart on the same sample are oriented in the same angle as shown in Figure S7. These results suggest that all MoS_2 layers in the film were epitaxially grown on the substrate in wafer scale, whereas the TVS growth of MoS_2 generally results in a polycrystalline film with rotational grains even on a crystalline substrate.[57] However, it remains unclear whether the film consists of a single grain or multiple grains with a mirror twin GB because both can produce a single set of hexagonal spots in their electron diffraction patterns. Here, the hexagonal spots can be divided into two families, namely, $[\bar{1}100]$ and $[1\bar{1}00]$, since the MoS_2 crystal possesses a three-fold rotational symmetry. They are known to have a slight difference in their spot intensity that could be used to distinguish the crystal orientation of twinned grains (rotated 60 or 180° with respect to each other).[58] However, this method can no longer be used for multilayered 2H-MoS_2 because the two layers in the stacking unit cell are inversely oriented, which is expected to break the three-fold symmetry and consequently produce hexagonal spots with an equivalent intensity. In fact, little difference was found in the spot intensity in our observation. Therefore, while the crystalline nature of the film is difficult to determine from the experimental results, we suppose that the film consists of twinned grains for two reasons: (1) MoS_2 has been found to have an epitaxial relationship with the sapphire surface, giving rise to two preferential orientations related by 60° rotation.[27] Considering the theoretical prediction reported that MoS_2 aligned along its preferential orientations grows by almost the same amount on the sapphire substrate,[59] this should be the case with our TVS-grown film. (2) There have been reports that the electrical properties of MoS_2 are much less affected by the mirror twin GBs than by the tilt GBs.[60,61] The electrical properties of our film were poorer than those of the CVD-grown film but still better than those of the previously reported TVS-grown films. This could be explained if our TVS-grown film is assumed to be composed of the twinned grains. Although we could not directly observe the atomically resolved image of twin GBs by TEM, a certain number of line defects were found in the lattice images where the MoS_2 crystal structure is distorted (Figure S8). This seems to be due to the presence of twin GBs in the topmost MoS_2 layer.

We propose the structure models of MoS_2 with and without the twin GB and perform first-principles calculations to explore

https://doi.org/10.1021/acsomega.1c05113
ACS Omega 2022, 7, 1851−1860

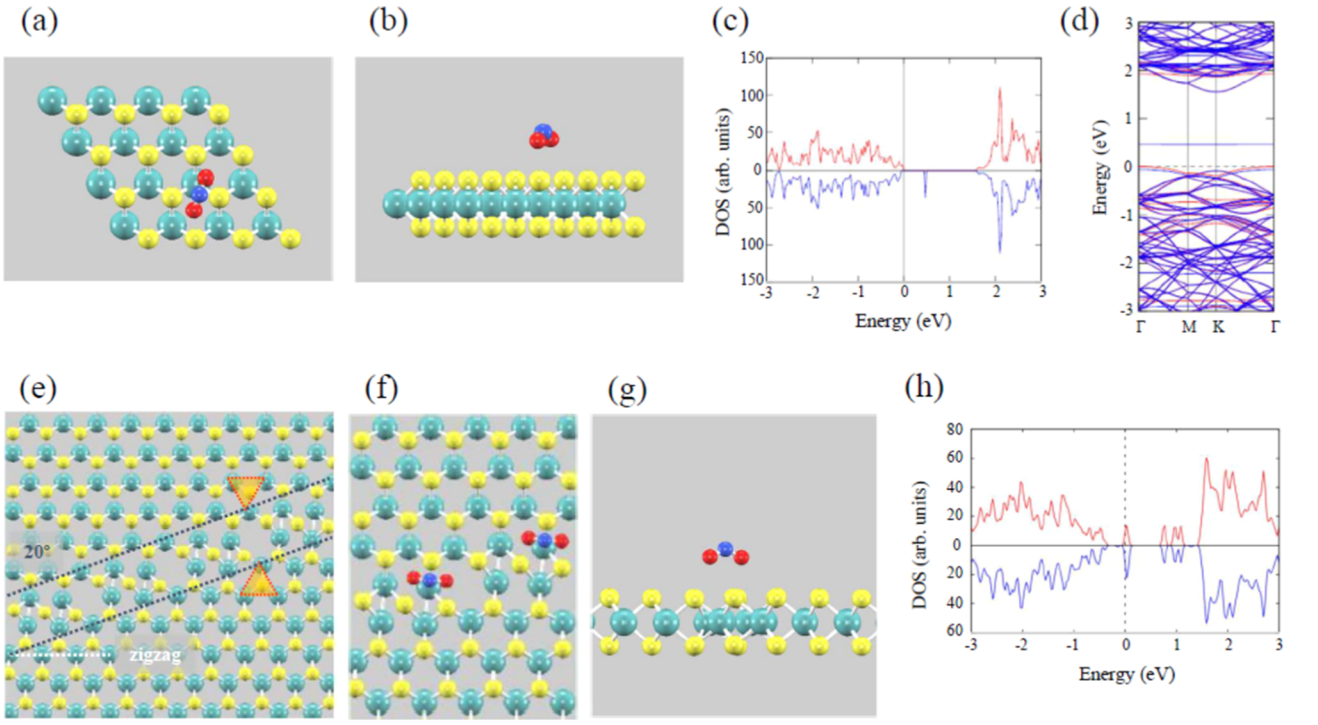

Figure 5. (a) Top and (b) side views of the most favorable configuration for NO_2 on ideal MoS_2. (c,d) The corresponding DOS and the band structure for the model shown in (a,b). (e) Model of MoS_2 with the twin GB (between dashed lines). Triangles are shown as a guide to see the orientation of MoS_2 grains. (f) Top and (g) side views of the most favorable configuration for NO_2 on the twin GB shown in (e). (h) The corresponding DOS for the model shown in (f,g). The red (blue) lines in (c,d,h) correspond to the up-spin (down-spin) states, and the dashed line denotes the Fermi level.

the NO_2 adsorption behavior on the surface. In addition, the charge transfer between MoS_2 and the adsorbed NO_2 molecule is compared for both models. Details of the calculation are described in the Methods section. Figure 5a,b shows the most stable adsorption configuration of NO_2 on an ideal MoS_2 surface. The configuration of this model is in good agreement with previous theoretical results.[62] The adsorption energy (E_a) for this model is determined to be 0.202 eV. All the models that we considered are summarized with the corresponding adsorption energies in Figure S9. The models in which NO_2 oriented toward MoS_2 with the O atom pointing down are commonly found to be stable for each adsorption site. To investigate the electronic properties of the most stable configuration, the total density of states (DOS) and the electronic band structure are analyzed. As shown in Figure 5c,d, an unoccupied state located 0.5 eV above the valence band maximum (VBM) is introduced by adsorbed NO_2,[62,63] as can be seen from the comparison with that of ideal MoS_2 before NO_2 adsorption (Figure S10). Then, Bader analysis is performed to estimate the charge-transfer value. The adsorbed NO_2 is found to accept 0.11e from MoS_2, indicating hole doping induced by NO_2, and well explains the experimental results.

Next, we constructed the model of MoS_2 with a twin GB as shown in Figure 5e by referring to the atomic structure that is commonly observed in previous TEM observations.[58,61] Two grains rotated 60° from one another are connected at the boundary at 20° off of the zigzag direction of MoS_2. The boundary is formed from periodic 4- and 8-membered rings whose periodicity varies in accordance with the angle relative to the zigzag direction. The most favorable configuration of NO_2 on the twin GB is shown in Figure 5f,g. The others considered for the calculation are summarized in Figure S11 for comparison. It is found that E_a strongly depends on the adsorption site on the GB, which sharply contrasts to the ideal surface. This implies that the sensing properties are strongly affected by the presence of the GB depending on its atomic configuration. The DOS shows that localized states are created around 0 and 1 eV within the band gap of ideal MoS_2. They are attributed to the structural defects in the twin GB, causing an upward shift of the Fermi level due to the n-doping effect of the periodic 8-4-4 ring structure.[58] On the other hand, the adsorbed NO_2 state is introduced at ∼0.5 eV above the VBM as is the case of the ideal surface, whereas it is obscured by the presence of the defect states. The most stable adsorption site gives the E_a of 0.217 eV, which is slightly larger than the value for the case of the ideal surface. It derives a charge-transfer value of 0.11e, which is comparable to that on the ideal surface. Therefore, it turned out that an equal amount of hole doping can occur even on a polycrystalline MoS_2 consisting of multiple twin grains. A large MoS_2 grain is not always necessary for the sensor to be able to detect NO_2 with high sensitivity, which supports the validity of our experimental results.

Another possible reason for higher sensitivity in the TVS-grown film than in the CVD-grown one is the high adsorption of NO_2 onto the edge sites of the film. The TVS-grown film exhibits a characteristic feature of many nanometer-sized pores that appear as dark in the STEM annular dark-field image (Figure S12). Enhancement of NO_2 adsorption properties along the edge sites has been reported to explain the superior response in a vertically aligned MoS_2 film compared with the horizontally aligned one.[64] A considerable amount of edge sites present in our porous film could also play a significant role in detecting NO_2 adsorption, resulting in enhancing the sensor

https://doi.org/10.1021/acsomega.1c05113
ACS Omega 2022, 7, 1851−1860

performance. The gas adsorption behavior on the tilt GB between rotational grains, which is more typical for a polycrystalline MoS_2 film, will also need to be further studied to clarify the effect of crystallinity on gas sensing properties from the sensor application point of view.

CONCLUSIONS

We demonstrated the comparative study of the NO_2 sensing capability of MoS_2 synthesized by CVD and TVS methods. The Langmuir isotherm model well described the NO_2 adsorption behavior on the MoS_2 surface that we observed. Although the TVS-grown film has electrical properties inferior to those of the CVD-grown one, the responsivity of the sensor is found to be higher for the former rather than for the latter. From TEM observations, it was supposed that the TVS-grown film is polycrystalline consisting of rotationally oriented twin grains. Theoretical calculation revealed that the NO_2 adsorption on the twin GB that we assumed was estimated to be comparable to that on the ideal basal plane surface. In addition, the edge sites, which are present in the porous structure of the TVS-grown film, could possibly play a crucial role in enhancing the adsorption property, leading to a rise in sensor response to NO_2. The findings of this study provide new insights into developing chemical sensors using MoS_2 and other two-dimensional materials.

ASSOCIATED CONTENT

Supporting Information

The Supporting Information is available free of charge at https://pubs.acs.org/doi/10.1021/acsomega.1c05113.

Raman spectra, XPS, TEM results, calculated models and the corresponding adsorption energies, DOS and band structure of MoS_2, and comparison of the reported MoS_2-based sensors for NO_2 detection (PDF)

AUTHOR INFORMATION

Corresponding Authors

Kenjiro Hayashi − *Fujitsu Laboratories Ltd., Atsugi, Kanagawa 243-0197, Japan; Fujitsu Limited, Kawasaki, Kanagawa 211-8588, Japan;* orcid.org/0000-0002-2287-0491; Email: hayashi.kenjiro@fujitsu.com

Shintaro Sato − *Fujitsu Laboratories Ltd., Atsugi, Kanagawa 243-0197, Japan; Fujitsu Limited, Kawasaki, Kanagawa 211-8588, Japan*; Email: sato.shintaro@fujitsu.com

Authors

Masako Kataoka − *Fujitsu Laboratories Ltd., Atsugi, Kanagawa 243-0197, Japan*

Hideyuki Jippo − *Fujitsu Laboratories Ltd., Atsugi, Kanagawa 243-0197, Japan; Fujitsu Limited, Kawasaki, Kanagawa 211-8588, Japan*

Junichi Yamaguchi − *Fujitsu Laboratories Ltd., Atsugi, Kanagawa 243-0197, Japan; Fujitsu Limited, Kawasaki, Kanagawa 211-8588, Japan*

Mari Ohfuchi − *Fujitsu Laboratories Ltd., Atsugi, Kanagawa 243-0197, Japan; Fujitsu Limited, Kawasaki, Kanagawa 211-8588, Japan;* orcid.org/0000-0001-6360-5726

Complete contact information is available at: https://pubs.acs.org/10.1021/acsomega.1c05113

Notes

The authors declare no competing financial interest.

ACKNOWLEDGMENTS

This research was partly supported by JST CREST grant number JPMJCR15F1, Japan.

REFERENCES

(1) Gong, C.; Zhang, H.; Wang, W.; Colombo, L.; Wallace, R. M.; Cho, K. Band alignment of two-dimensional transition metal dichalcogenides: Application in tunnel field effect transistors. *Appl. Phys. Lett.* **2013**, *103*, 053513.

(2) Ma, L.; Nath, D. N.; Lee, E. W.; Lee, C. H.; Yu, M.; Arehart, A.; Rajan, S.; Wu, Y. Epitaxial growth of large area single-crystalline few-layer MoS2 with high space charge mobility of 192cm2V−1 s−1. *Appl. Phys. Lett.* **2014**, *105*, 072105.

(3) Nourbakhsh, A.; Zubair, A.; Sajjad, R. N.; Amir Tavakkoli, K. G.; Chen, W.; Fang, S.; Ling, X.; Kong, J.; Dresselhaus, M. S.; Kaxiras, E.; Berggren, K. K.; Antoniadis, D.; Palacios, T. MoS2 Field-Effect Transistor with Sub-10 nm Channel Length. *Nano Lett.* **2016**, *16*, 7798−7806.

(4) Perkins, F. K.; Friedman, A. L.; Cobas, E.; Campbell, P. M.; Jernigan, G. G.; Jonker, B. T. Chemical Vapor Sensing with Monolayer MoS2. *Nano Lett.* **2013**, *13*, 668−673.

(5) He, Q.; Zeng, Z.; Yin, Z.; Li, H.; Wu, S.; Huang, X.; Zhang, H. Fabrication of Flexible MoS2 Thin-Film Transistor Arrays for Practical Gas-Sensing Applications. *Small* **2012**, *8*, 2994−2999.

(6) Li, H.; Yin, Z.; He, Q.; Li, H.; Huang, X.; Lu, G.; Fam, D. W. H.; Tok, A. I. Y.; Zhang, Q.; Zhang, H. Fabrication of Single- and Multilayer MoS2 Film-Based Field-Effect Transistors for Sensing NO at Room Temperature. *Small* **2012**, *8*, 63−67.

(7) Samnakay, R.; Jiang, C.; Rumyantsev, S. L.; Shur, M. S.; Balandin, A. A. Selective chemical vapor sensing with few-layer MoS2 thin-film transistors: Comparison with graphene devices. *Appl. Phys. Lett.* **2015**, *106*, 023115.

(8) Cho, B.; Hahm, M. G.; Choi, M.; Yoon, J.; Kim, A. R.; Lee, Y.-J.; Park, S.-G.; Kwon, J.-D.; Kim, C. S.; Song, M.; Jeong, Y.; Nam, K.-S.; Lee, S.; Yoo, T. J.; Kang, C. G.; Lee, B. H.; Ko, H. C.; Ajayan, P. M.; Kim, D.-H. Charge-transfer-based Gas Sensing Using Atomic-layer MoS2. *Sci. Rep.* **2015**, *5*, 8052.

(9) Late, D. J.; Huang, Y.-K.; Liu, B.; Acharya, J.; Shirodkar, S. N.; Luo, J.; Yan, A.; Charles, D.; Waghmare, U. V.; Dravid, V. P.; Rao, C. N. R. Sensing Behavior of Atomically Thin-Layered MoS2 Transistors. *ACS Nano* **2013**, *7*, 4879−4891.

(10) Cho, B.; Kim, A. R.; Park, Y.; Yoon, J.; Lee, Y.-J.; Lee, S.; Yoo, T. J.; Kang, C. G.; Lee, B. H.; Ko, H. C.; Kim, D.-H.; Hahm, M. G. Bifunctional Sensing Characteristics of Chemical Vapor Deposition Synthesized Atomic-Layered MoS2. *ACS Appl. Mater. Interfaces* **2015**, *7*, 2952−2959.

(11) Liu, B.; Chen, L.; Liu, G.; Abbas, A. N.; Fathi, M.; Zhou, C. High-Performance Chemical Sensing Using Schottky-Contacted Chemical Vapor Deposition Grown Monolayer MoS2 Transistors. *ACS Nano* **2014**, *8*, 5304−5314.

(12) Lee, Y.; Lee, J.; Bark, H.; Oh, I.-K.; Ryu, G. H.; Lee, Z.; Kim, H.; Cho, J. H.; Ahn, J.-H.; Lee, C. Synthesis of wafer-scale uniform molybdenum disulfide films with control over the layer number using a gas phase sulfur precursor. *Nanoscale* **2014**, *6*, 2821−2826.

(13) Liu, H.; Ansah Antwi, K. K.; Ying, J.; Chua, S.; Chi, D. Towards large area and continuous MoS2 atomic layers via vapor-phase growth: thermal vapor sulfurization. *Nanotechnology* **2014**, *25*, 405702.

(14) Lee, K.; Gatensby, R.; McEvoy, N.; Hallam, T.; Duesberg, G. S. High-Performance Sensors Based on Molybdenum Disulfide Thin Films. *Adv. Mater.* **2013**, *25*, 6699−6702.

(15) Yin, Z.; Li, H.; Li, H.; Jiang, L.; Shi, Y.; Sun, Y.; Lu, G.; Zhang, Q.; Chen, X.; Zhang, H. Single-Layer MoS2 Phototransistors. *ACS Nano* **2012**, *6*, 74−80.

(16) Furchi, M. M.; Polyushkin, D. K.; Pospischil, A.; Mueller, T. Mechanisms of Photoconductivity in Atomically Thin MoS2. *Nano Lett.* **2014**, *14*, 6165−6170.

(17) Wang, Y.; He, Z.; Zhang, J.; Liu, H.; Lai, X.; Liu, B.; Chen, Y.; Wang, F.; Zhang, L. UV illumination enhanced desorption of oxygen molecules from monolayer MoS2 surface. *Nano Res.* **2020**, *13*, 358−365.
(18) Han, P.; Adler, E. R.; Liu, Y.; St Marie, L.; El Fatimy, A.; Melis, S.; Van Keuren, E.; Barbara, P. Ambient effects on photogating in MoS2 photodetectors. *Nanotechnology* **2019**, *30*, 284004.
(19) Pham, T.; Li, G.; Bekyarova, E.; Itkis, M. E.; Mulchandani, A. MoS2-Based Optoelectronic Gas Sensor with Sub-parts-per-billion Limit of NO2 Gas Detection. *ACS Nano* **2019**, *13*, 3196−3205.
(20) Xia, Y.; Hu, C.; Guo, S.; Zhang, L.; Wang, M.; Peng, J.; Xu, L.; Wang, J. Sulfur-Vacancy-Enriched MoS2 Nanosheets Based Heterostructures for Near-Infrared Optoelectronic NO2 Sensing. *ACS Appl. Nano Mater.* **2020**, *3*, 665−673.
(21) Reina, A.; Son, H.; Jiao, L.; Fan, B.; Dresselhaus, M. S.; Liu, Z.; Kong, J. Transferring and Identification of Single- and Few-Layer Graphene on Arbitrary Substrates. *J. Phys. Chem. C* **2008**, *112*, 17741−17744.
(22) Hayashi, K.; Kataoka, M.; Jippo, H.; Ohfuchi, M.; Sato, S. Vacancy-Assisted Selective Detection of Low-ppb Formaldehyde in Two-Dimensional Layered SnS2. *ACS Appl. Mater. Interfaces* **2020**, *12*, 12207−12214.
(23) See the web site of PHASE system software [https://azuma.nims.go.jp] (accessed April 12, 2021).
(24) Perdew, J. P.; Burke, K.; Ernzerhof, M. Generalized Gradient Approximation Made Simple. *Phys. Rev. Lett.* **1996**, *77*, 3865−3868.
(25) Grimme, S. Semiempirical GGA-type density functional constructed with a long-range dispersion correction. *J. Comput. Chem.* **2006**, *27*, 1787−1799.
(26) Lee, Y.-H.; Zhang, X.-Q.; Zhang, W.; Chang, M.-T.; Lin, C.-T.; Chang, K.-D.; Yu, Y.-C.; Wang, J. T.-W.; Chang, C.-S.; Li, L.-J.; Lin, T.-W. Synthesis of Large-Area MoS2 Atomic Layers with Chemical Vapor Deposition. *Adv. Mater.* **2012**, *24*, 2320−2325.
(27) Dumcenco, D.; Ovchinnikov, D.; Marinov, K.; Lazić, P.; Gibertini, M.; Marzari, N.; Sanchez, O. L.; Kung, Y.-C.; Krasnozhon, D.; Chen, M.-W.; Bertolazzi, S.; Gillet, P.; Fontcuberta i Morral, A.; Radenovic, A.; Kis, A. Large-Area Epitaxial Monolayer MoS2. *ACS Nano* **2015**, *9*, 4611−4620.
(28) Jiménez Sandoval, S.; Yang, D.; Frindt, R. F.; Irwin, J. C. Raman study and lattice dynamics of single molecular layers of MoS2. *Phys. Rev. B: Condens. Matter Mater. Phys.* **1991**, *44*, 3955−3962.
(29) Mignuzzi, S.; Pollard, A. J.; Bonini, N.; Brennan, B.; Gilmore, I. S.; Pimenta, M. A.; Richards, D.; Roy, D. Effect of disorder on Raman scattering of single-layer MoS2. *Phys. Rev. B: Condens. Matter Mater. Phys.* **2015**, *91*, 195411.
(30) Baek, S. H.; Choi, Y.; Choi, W. Large-Area Growth of Uniform Single-Layer MoS2 Thin Films by Chemical Vapor Deposition. *Nanoscale Res. Lett.* **2015**, *10*, 388.
(31) Zafar, A.; Nan, H.; Zafar, Z.; Wu, Z.; Jiang, J.; You, Y.; Ni, Z. Probing the intrinsic optical quality of CVD grown MoS2. *Nano Res.* **2017**, *10*, 1608−1617.
(32) Li, H.; Zhang, Q.; Yap, C. C. R.; Tay, B. K.; Edwin, T. H. T.; Olivier, A.; Baillargeat, D. From Bulk to Monolayer MoS2: Evolution of Raman Scattering. *Adv. Funct. Mater.* **2012**, *22*, 1385−1390.
(33) Lee, C.; Yan, H.; Brus, L. E.; Heinz, T. F.; Hone, J.; Ryu, S. Anomalous Lattice Vibrations of Single- and Few-Layer MoS2. *ACS Nano* **2010**, *4*, 2695−2700.
(34) Radisavljevic, B.; Radenovic, A.; Brivio, J.; Giacometti, V.; Kis, A. Single-layer MoS2 transistors. *Nat. Nanotechnol.* **2011**, *6*, 147−150.
(35) Wu, W.; De, D.; Chang, S.-C.; Wang, Y.; Peng, H.; Bao, J.; Pei, S.-S. High mobility and high on/off ratio field-effect transistors based on chemical vapor deposited single-crystal MoS2 grains. *Appl. Phys. Lett.* **2013**, *102*, 142106.
(36) Kwon, H.; Garg, S.; Park, J. H.; Jeong, Y.; Yu, S.; Kim, S. M.; Kung, P.; Im, S. Monolayer MoS2 field-effect transistors patterned by photolithography for active matrix pixels in organic light-emitting diodes. *npj 2D Mater. Appl.* **2019**, *3*, 9.
(37) Zhang, Y.; Kolmakov, A.; Chretien, S.; Metiu, H.; Moskovits, M. Control of Catalytic Reactions at the Surface of a Metal Oxide Nanowire by Manipulating Electron Density Inside It. *Nano Lett.* **2004**, *4*, 403−407.
(38) Kang, Y.; Pyo, S.; Jo, E.; Kim, J. Light-assisted recovery of reacted MoS2 for reversible NO2 sensing at room temperature. *Nanotechnology* **2019**, *30*, 355504.
(39) Kumar, R.; Goel, N.; Kumar, M. UV-Activated MoS2 Based Fast and Reversible NO2 Sensor at Room Temperature. *ACS Sens.* **2017**, *2*, 1744−1752.
(40) Wieting, T. J.; Verble, J. L. Infrared and Raman Studies of Long-Wavelength Optical Phonons in Hexagonal MoS2. *Phys. Rev. B: Condens. Matter Mater. Phys.* **1971**, *3*, 4286−4292.
(41) Nayak, A. P.; Pandey, T.; Voiry, D.; Liu, J.; Moran, S. T.; Sharma, A.; Tan, C.; Chen, C.-H.; Li, L.-J.; Chhowalla, M.; Lin, J.-F.; Singh, A. K.; Akinwande, D. Pressure-Dependent Optical and Vibrational Properties of Monolayer Molybdenum Disulfide. *Nano Lett.* **2015**, *15*, 346−353.
(42) Liu, K.-K.; Zhang, W.; Lee, Y.-H.; Lin, Y.-C.; Chang, M.-T.; Su, C.-Y.; Chang, C.-S.; Li, H.; Shi, Y.; Zhang, H.; Lai, C.-S.; Li, L.-J. Growth of Large-Area and Highly Crystalline MoS2 Thin Layers on Insulating Substrates. *Nano Lett.* **2012**, *12*, 1538−1544.
(43) Choudhary, N.; Park, J.; Hwang, J. Y.; Choi, W. Growth of Large-Scale and Thickness-Modulated MoS2 Nanosheets. *ACS Appl. Mater. Interfaces* **2014**, *6*, 21215−21222.
(44) Laskar, M. R.; Ma, L.; Kannappan, S.; Sung Park, P.; Krishnamoorthy, S.; Nath, D. N.; Lu, W.; Wu, Y.; Rajan, S. Large area single crystal (0001) oriented MoS2. *Appl. Phys. Lett.* **2013**, *102*, 252108.
(45) Tarasov, A.; Campbell, P. M.; Tsai, M.-Y.; Hesabi, Z. R.; Feirer, J.; Graham, S.; Ready, W. J.; Vogel, E. M. Highly Uniform Trilayer Molybdenum Disulfide for Wafer-Scale Device Fabrication. *Adv. Funct. Mater.* **2014**, *24*, 6389−6400.
(46) Vangelista, S.; Cinquanta, E.; Martella, C.; Alia, M.; Longo, M.; Lamperti, A.; Mantovan, R.; Basset, F. B.; Pezzoli, F.; Molle, A. Towards a uniform and large-scale deposition of MoS2 nanosheets via sulfurization of ultra-thin Mo-based solid films. *Nanotechnology* **2016**, *27*, 175703.
(47) Zheng, J.; Yan, X.; Lu, Z.; Qiu, H.; Xu, G.; Zhou, X.; Wang, P.; Pan, X.; Liu, K.; Jiao, L. High-Mobility Multilayered MoS2 Flakes with Low Contact Resistance Grown by Chemical Vapor Deposition. *Adv. Mater.* **2017**, *29*, 1604540.
(48) Young, J. R.; Chilcote, M.; Barone, M.; Xu, J.; Katoch, J.; Luo, Y. K.; Mueller, S.; Asel, T. J.; Fullerton-Shirey, S. K.; Kawakami, R.; Gupta, J. A.; Brillson, L. J.; Johnston-Halperin, E. Uniform large-area growth of nanotemplated high-quality monolayer MoS2. *Appl. Phys. Lett.* **2017**, *110*, 263103.
(49) Chen, J.; Tang, W.; Tian, B.; Liu, B.; Zhao, X.; Liu, Y.; Ren, T.; Liu, W.; Geng, D.; Jeong, H. Y.; Shin, H. S.; Zhou, W.; Loh, K. P. Chemical Vapor Deposition of High-Quality Large-Sized MoS2 Crystals on Silicon Dioxide Substrates. *Adv. Sci.* **2016**, *3*, 1500033.
(50) Zhan, Y.; Liu, Z.; Najmaei, S.; Ajayan, P. M.; Lou, J. Large-Area Vapor-Phase Growth and Characterization of MoS2 Atomic Layers on a SiO2 Substrate. *Small* **2012**, *8*, 966−971.
(51) Robertson, J.; Liu, X.; Yue, C.; Escarra, M.; Wei, J. Wafer-scale synthesis of monolayer and few-layer MoS 2 via thermal vapor sulfurization. *2D Mater.* **2017**, *4*, 045007.
(52) Qiu, H.; Pan, L.; Yao, Z.; Li, J.; Shi, Y.; Wang, X. Electrical characterization of back-gated bi-layer MoS2 field-effect transistors and the effect of ambient on their performances. *Appl. Phys. Lett.* **2012**, *100*, 123104.
(53) Late, D. J.; Liu, B.; Matte, H. S. S. R.; Dravid, V. P.; Rao, C. N. R. Hysteresis in Single-Layer MoS2 Field Effect Transistors. *ACS Nano* **2012**, *6*, 5635−5641.
(54) Park, W.; Park, J.; Jang, J.; Lee, H.; Jeong, H.; Cho, K.; Hong, S.; Lee, T. Oxygen environmental and passivation effects on molybdenum disulfide field effect transistors. *Nanotechnology* **2013**, *24*, 095202.
(55) Zhang, F.; Momeni, K.; AlSaud, M. A.; Azizi, A.; Hainey, M. F.; Redwing, J. M.; Chen, L.-Q.; Alem, N. Controlled synthesis of 2D

https://doi.org/10.1021/acsomega.1c05113
ACS Omega 2022, 7, 1851−1860

transition metal dichalcogenides: from vertical to planar MoS 2. *2D Mater* **2017**, *4*, 025029.
(56) Chen, J.; Zhao, X.; Grinblat, G.; Chen, Z.; Tan, S. J. R.; Fu, W.; Ding, Z.; Abdelwahab, I.; Li, Y.; Geng, D.; Liu, Y.; Leng, K.; Liu, B.; Liu, W.; Tang, W.; Maier, S. A.; Pennycook, S. J.; Loh, K. P. Homoepitaxial Growth of Large-Scale Highly Organized Transition Metal Dichalcogenide Patterns. *Adv. Mater.* **2018**, *30*, 1704674.
(57) Orofeo, C. M.; Suzuki, S.; Sekine, Y.; Hibino, H. Scalable synthesis of layer-controlled WS2 and MoS2 sheets by sulfurization of thin metal films. *Appl. Phys. Lett.* **2014**, *105*, 083112.
(58) van der Zande, A. M.; Huang, P. Y.; Chenet, D. A.; Berkelbach, T. C.; You, Y.; Lee, G.-H.; Heinz, T. F.; Reichman, D. R.; Muller, D. A.; Hone, J. C. Grains and grain boundaries in highly crystalline monolayer molybdenum disulphide. *Nat. Mater.* **2013**, *12*, 554−561.
(59) Jippo, H.; Hayashi, K.; Sato, S.; Ohfuchi, M. Stability of two orientations of MoS2 on α-Al2O3(0001). *Jpn. J. Appl. Phys.* **2017**, *56*, 105701.
(60) Najmaei, S.; Amani, M.; Chin, M. L.; Liu, Z.; Birdwell, A. G.; O'Regan, T. P.; Ajayan, P. M.; Dubey, M.; Lou, J. Electrical Transport Properties of Polycrystalline Monolayer Molybdenum Disulfide. *ACS Nano* **2014**, *8*, 7930−7937.
(61) Ly, T. H.; Perello, D. J.; Zhao, J.; Deng, Q.; Kim, H.; Han, G. H.; Chae, S. H.; Jeong, H. Y.; Lee, Y. H. Misorientation-angle-dependent electrical transport across molybdenum disulfide grain boundaries. *Nat. Commun.* **2016**, *7*, 10426.
(62) Zhao, S.; Xue, J.; Kang, W. Gas adsorption on MoS2 monolayer from first-principles calculations. *Chem. Phys. Lett.* **2014**, *595*−*596*, 35−42.
(63) Yue, Q.; Shao, Z.; Chang, S.; Li, J. Adsorption of gas molecules on monolayer MoS2 and effect of applied electric field. *Nanoscale Res. Lett.* **2013**, *8*, 425.
(64) Cho, S.-Y.; Kim, S. J.; Lee, Y.; Kim, J.-S.; Jung, W.-B.; Yoo, H.-W.; Kim, J.; Jung, H.-T. Highly Enhanced Gas Adsorption Properties in Vertically Aligned MoS2 Layers. *ACS Nano* **2015**, *9*, 9314−9321.

https://doi.org/10.1021/acsomega.1c05113
ACS Omega 2022, 7, 1851−1860